APPENDIX

Geology of the four major historical vermiculite ore deposits

Three principal types of vermiculite ore deposits occur in similar but distinct petrologic environments (Bush 1976). Type 1 deposits form in large, sometimes zoned, ultramafic pyroxenite intrusions cut by syenite or alkali granite, carbonatitic, and pegmatite intrusions. Type 2 deposits form in small to large dunite and unzoned pyroxenite and peridotite intrusives, cut by pegmatite, syenitic, or granitic rocks. Type 3 deposits form in metamorphosed ultramafic rocks (e.g., amphibole schist), some of which are cut by or in contact with pyroxenite or peridotite and cut by pegmatite (Bush 1976). Both Libby and Palabora are type 1 deposits; Louisa is a type 3 deposit (Bush 1976), whereas Enoree has type 2 and 3 deposits.

The Zonolite Mountain vermiculite mine is located 12 km NE of the town of Libby, Montana (Fig. A3), and is within the Rainy Creek Complex, a hydrothermally altered ultramafic intrusion of Cretaceous age. The Rainy Creek Complex consists of inwardly arranged concentric zones of magnetite pyroxenite, biotite pyroxenite and biotitite (a rock composed almost entirely of Al-Fe phlogopite). Numerous dikes of alkaline syenite and granite, trachyte-phonolite, pegmatite, and quartz-rich veins cut these zones (Pardee and Larsen 1928; Bassett 1959; Boettcher 1967). Hydrothermal fluids that converted pyroxene to sodic-calcic elongate amphibole altered rocks close to pegmatite veins; recent supergene weathering at or near the surface converted Al-Fe phlogopite to hydrobiotite and vermiculite.

Vermiculite ore is still mined from the three other major historical sources. Production from the Louisa deposit began in 1978 from a 24- to 30-m thick weathered zone in the Ordovician Green Springs pluton and is still in operation (Virginia DMME 2012). Here, the Virginia Vermiculite mine excavates a complexly zoned package of ultramafic rocks, mainly composed of micaceous pyroxenites and amphibolites cut by thin felsic dikes. Vermiculite ore is purified at a mill on the mine property. According to references cited by Frank and Edmond (2001), amphibole and chrysotile "fibers" were found in all six of the Louisa vermiculite ore samples examined by Rohl and Langer (1977).

Numerous vermiculite ore deposits near Enoree, South Carolina, are hosted in biotitite units in metamorphosed potassic ultramafic intrusions cut by pegmatites (Libby 1975). Vermiculite ore production began in the district at Tigerville, South Carolina, in 1937 (Bush and Sweeney 1968). Libby (1975) found that amphibole "asbestos" is associated with some vermiculite ore deposits in the Enoree district. Atkinson et al. (1982) found "fiber"-producing amphibole bundles at the mills processing this vermiculite ore.

The Palabora vermiculite ore deposit near Phalaborwa, South Africa, began production in 1946 from a coarse-grained zoned Proterozoic ultramafic unit of phlogopite-serpentine surrounded by phlogopite-diopside, in which, phlogopite in the weathered zone is altered to "hydrophlogopite" and vermiculite (Palabora Mining Company 1976; Muiambo 2011). Moatamed et al. (1986) found short "fibrous structures" in expanded Palabora vermiculite ore and 0.4% "fibrous" amphibole in unexpanded ore samples.

Unexpanded vermiculite ore usually undergoes a series of processing steps at the mine sites, where crude ore from open-pit mines is screened to remove waste rock. After this step, ore is typically separated into fractions by wet screening, then dewatered, dried, and classified as part of the beneficiation process (Hindman, 2006). Sized and beneficiated unexpanded vermiculite ore is distributed by rail or truck to various thermal expansion plants around the U.S.A. and Canada.

Continuum removal of spectral absorptions

It can be visually difficult to compare the precise shapes, depths, and wavelength positions of the narrow vibrational absorptions, especially when they are overwhelmed by broad overlapping Fe-electronic absorptions that vary in intensity depending on the composition of a given vermiculite ore sample. Fortunately, absorptions can be normalized for direct comparison of wavelength positions regardless of original continuum slope, reflectance level, and intensity. As shown by Clark and Roush (1984) and Clark (1999), this approach calculates the band depth by first normalizing a diagnostic absorption (e.g., the 1.38 μm absorption) for variations in continuum slope and spectral intensity (Fig. A4). This is accomplished by dividing the reflectance value of each spectral channel in an absorption by the corresponding reflectance value of a continuum drawn between endpoints on the shoulders of the absorption (Figs. A4b and A4c). The minimum channel of the continuum-removed data is found between the continuum endpoints, and a parabola is statistically fit to it and the two channels nearest to this minimum. The reflectance of the parabola's center wavelength is determined, and then subtracted from 1.00 to derive the band depth of the absorption (Fig. A4d), as implemented in the "interactive band analysis" routine in the SPECPR program (Clark 1993) and "continuum-removal GUI" in the PRISM plugin (Kokaly 2011) for ENVI® image-processing software. Doing the same for all diagnostic absorptions in a spectrum provides a quantitative way to compare "continuum-removed" spectral features of expanded vermiculite ore samples based on derived parameters such as band center position, FWHM, continuum-removed depth, and band asymmetry.

Additional cation-exchange experiments

Additional K^+-exchange experiments were performed on an expanded ore sample to determine if the type of cation present in the interlayer site influenced the 3647 cm^{-1} absorption. One split of the expanded ALB22SC00 ore from Enoree, South Carolina, was treated with a 1 M KCl solution for 43 hours at 100° C at a 1:10 solid:liquid weight ratio. After rinsing in DI water several times, this K^+-exchanged sample was allowed to dry for several

days and then measured in the mid-infrared (MIR) in KBr-pellet form on the Nicolet spectrometer. Figure A5 shows continuum-removed absorptions in spectra of the expanded sample and its K^+-exchanged counterpart in the OH stretch fundamental region and their deconvolution into symmetrical Gaussians. K^+ exchange eliminates the ν_h and ν_j $Mg_2(Fe^{3+}, Al, Ti)OH_{non\text{-}repulsed}$ absorptions due to partial replacement of interlayer water by K^+, causing increased repulsion of adjacent octahedral hydroxyl H atoms. In addition, the ν_a and ν_b $Mg_3OH_{repulsed}$ absorptions intensify relative to the ν_d and ν_e $Mg_3OH_{non\text{-}repulsed}$ absorptions as K^+ replaces adjacent interlayer water. Finally, the ν_1 3741 cm^{-1} absorption weakens as K^+ replaces interlayer cations with higher charges (e.g., Mg^{2+} and Ca^{2+}). Note that the relative intensity of the ν_3 MgAl□OH absorption at 3647 cm^{-1} remains constant compared to the ν_g repulsed I-band absorption regardless of cation exchange suggesting ν_3 is a non-repulsed I-band or a vacancy (V-band) absorption.

Compositional and spectral analysis of Mg-rich VTx-1 vermiculite

A MIR spectrum of an unexpanded Mg-rich vermiculite VTx-1 sample from Llano, Texas, also shows an absorption at 3648 cm^{-1} similar to that seen in spectra of expanded ore from the Louisa, Virginia; Enoree, South Carolina; and Libby, Montana historical sources, but lacks a non-repulsed ν_j I-band absorption and ν_i and ν_k $MgFe^{3+}$□OH V-band absorptions (Fig. A6a). Compositional analysis of the VTx-1 sample (Table A5) indicates very little Fe, implying that Mg and, to a lesser extent, Al dominate the octahedral cation clusters. In the sample, Fe occupies only up to 0.5% of the octahedral cation sites, whereas Al occupies 3% of those sites (or 1 Fe per 7 Al atoms). Given this low Fe/Al compositional distribution, it seems statistically more likely that the 3648 cm^{-1} absorption is a ν_3 MgAl□OH V-band absorption rather than a $MgFe^{3+}$□OH V-band absorption. The corresponding δ^3 out-of-plane cation-OH bend absorption is located at 831 cm^{-1} (Fig. A6b). This position is within the range for MgAl□OH bend absorptions determined by Gates (2005) for dioctahedral smectites. Coupled with the OH stretch, this bend should give rise to a combination absorption at 4446 cm^{-1} (2.249 μm) with a 33 cm^{-1} anharmonicity correction, a wavelength position remarkably close to the 2.245 μm absorption seen in near-infrared (NIR) reflectance spectra of the VTx-1 sample (Fig. A7a).

In a comparison of unexpanded VTx-1 vermiculite spectra, the 2.24 μm absorption retains it intensity after K^+ exchange, indicating it is not a non-repulsed absorption and that the OH giving rise to it is relatively independent of interactions with interlayer cations (Fig. A7a). Polarized spectra of VTx-1 flakes indicate that the 2.24 μm absorption progressively intensifies as the basal cleavage is rotated parallel (0° inclination) to the polarized light (bottom spectrum of Fig. A7b). These observations suggest that the 2.24 μm absorption in the VTx-1 sample is a V-band combination absorption with its O-H bonds oriented nearly parallel to the layers, and in this case forms naturally (i.e., not requiring heat-induced expansion as it does in the commercial vermiculite ores from the major historical sources).

As an experiment, a ground split of the VTx-1 sample was used to establish which absorptions were influenced by interlayer water. For deuteration, the split was placed in a closed vial with D_2O and heated in an oven for 72 hours at 50 °C then vacuum dried just prior to reflectance measurement. This procedure replaced most of the interlayer water with D_2O. Under these conditions, nearly all of the interlayer water that gives rise to broad H_2O-related composite absorptions spanning the range from 1.39 to 1.54 μm, is replaced by D_2O and its absorptions shifted to longer wavelengths (not shown), leaving only the OH-stretch-overtone composite absorption at 1.39 μm and a shoulder at 1.405 μm (middle spectrum of Fig. A8a). A separate sample split was placed in a Parr bomb capsule with D_2O and heated in an oven for 72 hours at 250 °C. This split was dried and its spectrum measured in reflectance. The bottom spectrum in Figure A8a shows that most of the OH is replaced by OD and the N- and I-band stretch overtone composite absorption at 1.39 μm is shifted to longer wavelengths (not shown), leaving the V-band absorption overtones near 1.405 μm to dominate this spectral region. The persistence of the MgAl□OH vacancy band is also evident in the 2 μm region where its corresponding combination absorption at 2.24 μm remains strong (Fig A8b). Evidently, the H atoms associated with this vacancy cation cluster have strong hydrogen bonds to neighboring apical tetrahedral O atoms so they are not as easily replaced by D atoms. Note that the increased depth of the 2.24 μm combination absorption, with progressive deuteration of susceptible hydroxyl hydrogens and resulting decline of N- and I-band absorptions at 2.30, 2.32, and 2.38 μm and interlayer water at 2.92 μm (3425 cm^{-1}; not shown), is a consequence of increasing photon path length through the sample caused by weakening of the neighboring OH and overlapping water absorptions.

Skewness test of impurity grain size distribution using the 1.40/1.42 μm band depth ratio

Although the degree of elongation of amphibole and serpentine particles in expanded vermiculite ore is not directly measurable using the 1.40/1.42 μm band depth ratio, this spectral parameter varies with the size of impurity particles. As a test of this concept, spectral measurements were made of vermiculite insulation GDS701 collected from an attic in Libby and of an expanded vermiculite ore – amphibole mixture prepared in the laboratory. The attic insulation contains 6 wt% amphibole based on sink fraction measurements, whereas the mixture was constructed by adding 5 wt% of Libby amphiboles to a split of the expanded GDS327 ore sample considered to contain almost no amphibole. Amphibole bundles in the Libby attic sample were 3 to 4 mm in length whereas the amphibole, used to make the mixture, consisted of disaggregated individual elongate particles with an average length of 5 μm. The 1.40/1.42 μm band-depth-ratio values were calculated for 44 and 19 individual spectral measurements of the attic and constructed mixture samples, respectively. Figure A9 shows a wide vertical spread of band-depth-ratio values for the Libby attic sample and a tighter cluster for the mixture sample. The degree of skewness and its sign can be used to characterize the distribution of band-depth-ratios values. Values for the Libby attic sample have a distribution with a large positive skewness (3.340), or right asymmetry, whereas values for the laboratory mixture have a distribution with a smaller negative skewness (-0.983). Differences in the skewness of 1.40/1.42 μm band-

depth-ratio-value distributions may be used as a rough guide for detecting large pieces or bundles of impurities. However, because these band-depth-ratio values do not indicate individual particle shape or necessarily detect smaller elongate particles (e.g., <100 microns in size) when they are mixed with large bundles, they cannot be used to evaluate potential respiratory hazards. Nonetheless, the 1.40/1.42 μm band depth ratios will, in most cases, indicate the presence of impurities such as amphibole, talc, and/or serpentine, especially when they are present as particles or bundles several millimeters in size.

Optimum number of spectral measurements for determining the source of vermiculite ore

The air-trapping quality of large flakes of expanded vermiculite ore makes them preferred for insulation. However, their large size relative to the spectrometer's fiber-optic field of view makes it more difficult to spectrally average out flake-to-flake compositional variations, which is necessary for accurate determination of an ore's source and detection of its impurities. Because expanded vermiculite ore is a heterogeneous mixture of phlogopite, hydrobiotite, and vermiculite at scales ranging from entire flakes down to zones within individual flakes, it is necessary to make enough spectral measurements so no one mica flake dominates an analysis. The ASD contact probe®, used for spectral measurements, covers a roughly 1-cm^2 area of the sample during each measurement. Each band-depth-ratio value plotted in Figure 16 is an average of 20 or more spectral reflectance measurements per sample for those with an adequate volume of material (i.e., insulation sample GDS460 was only measured 12 times because of its low ~50 cm^3 sample volume). Accordingly, expanded ores with relatively smaller flakes require fewer spectral measurements to average out mineralogical and compositional variations than do those with larger flakes.

The minimum surface area of expanded ore, which must be measured to derive repeatable band-depth-ratio values, can be determined by calculating the cumulative averages of band-depth-ratio values from individual measurements. Figure A10 shows individual and cumulative average 1.38/2.32 μm band-depth-ratio values for the expanded Libby GDS701 sample with flakes 4 to 5 mm across, and for the expanded Libby GDS653 sample with flakes 1 to 2 mm across. The individual band-depth-ratio values plot on the lower half of the Libby provenance field for the coarser sample, but are confined to the lower quarter of the plot for the finer sample (compare Figs. A10a and b). The progressive cumulative average values for the coarser sample shift entirely into the Libby provenance field, as more spectral measurements are averaged, achieving a stable value after completing enough measurements to cover 43 cm^2 of the sample's surface (Fig. A10c). In contrast, spectral measurement of only 20 cm^2 is required to characterize the finer sample (Fig. A10d). Evaluation for the presence of impurities using 1.40/1.42 μm band-depth-ratio values (Fig. A11), using the same samples, required measurement of 28 cm^2 to attain a stable value in the coarser sample, whereas measurement of only 20 cm^2 was required for the finer sample. Surprisingly, it takes spectral measurement of 100 cm^2 of the coarser sample surface to achieve stable values, whereas it takes measurement of 60 cm^2 to achieve stable values from the finer sample using the 2.24/2.38 μm band depth ratio (Fig. A12). The need for spectral analysis of a larger surface area to attain stable 2.24/2.38 μm band-depth-ratio values for both coarser- and finer-grained expanded vermiculite ores is due to the larger spread of individual band-depth-ratio values, which is attributed to greater Al compositional variation among the sample's mica flakes. Accordingly, source determination using spectral analysis of expanded vermiculite ores to determine their source requires measurement over the necessary minimum surface area for a reliable 2.24/2.38 μm band-depth-ratio determination.

Effects of UV-NIR spectrometer resolution on determining the source of vermiculite ore

The positions of the vermiculite ore provenance field boundaries, in the band-depth-ratio diagrams discussed in the "Vermiculite Source Determination" section of the paper, were empirically derived and are influenced by the spectral resolution of the ASD FieldPro® and FieldSpec® spectrometers used to measure the expanded ore samples. Specifically, the relatively narrow OH-overtone absorptions in the 1.40-μm region deepen as spectral resolution becomes finer while the depth of broad OH-stretch-plus-bend combination absorptions in the 2.3-μm region remain relatively unaffected. Spectral measurements made with instruments with finer resolution than those used in this study would result in larger band-depth-ratio values causing them to plot outside of their empirically determined provenance fields shown in Figure 16, and potentially lead to misidentification of the expanded vermiculite ore's source. The 2.24-μm composite absorption is relatively narrow so it is even more sensitive to the effects of finer spectral resolution, though it is not as sensitive to it as are the 1.40-μm region absorptions. Nonetheless, using finer resolution measurements of the 2.24 μm absorption can still lead to misidentification of an expanded ore's source when using the provenance fields shown in Figures 18 and 21. Therefore, application of the spectral identification methods described in this paper requires that reflectance spectra be collected at the same resolution (i.e., using a 2.1 nm sampling interval, resampled to 1 nm by the software, and 11 to 12 nm bandpass (FWHM) over the 1 to 2.5 μm spectral range) as that used to construct the provenance diagrams, or requires convolution of finer resolution spectra to that used in this study (e.g., using spectral software packages like the SPECPR program (Clark 1993) or the "continuum-removal GUI" in the PRISM plugin (Kokaly 2011) for ENVI® image-processing software). Confirming the accuracy of all spectral convolutions is a critical step when using the Vermiculite SPectral Evaluation and Classification (VSPEC) method. Figures A13 to A15 show that spectra of four expanded vermiculite ores, representative of their source locations, can be measured at finer resolution and then convolved to the resolution used to construct the provenance fields without much shift in their plotted band-depth-ratio values. Spectra collected using a coarser sampling interval and/or coarser bandpass cannot be accurately convolved to the resolution of the spectra used to construct the provenance diagrams shown in this paper. Additionally, the VSPEC method was calibrated using expanded vermiculite ores; it is likely that the provenance field boundaries may need to be adjusted when applying the spectral method to unexpanded ores.

Spectral comparison of saponite, vermiculite, and vermiculite ore

Saponite [$(Ca,Na)_{0.3}(Mg,Fe^{2+})_3(Si,Al)_4O_{10}(OH)_2 \cdot 4(H_2O)$] is a trioctahedral smectite that commonly forms in hydrothermal veins, basaltic vesicles, and serpentinites in terrestrial environments. It has tentatively been found on the surface of Mars (Mustard et al. 2008; Ehlmann et al. 2009), but questions remain as to whether the orbitally measured spectral features may actually be those of vermiculite (Carter et al. 2013). Figure A16 shows the overtone and combination absorptions in spectra of handpicked, ground vermiculite flakes from the Libby GDS469 ore, a Mg-rich saponite from Ballarat, California (SapCa-1 from the Source Clays Repository), and expanded vermiculite ore GDS909 from Libby.

Saponite shares many spectral similarities with vermiculite as expected because their compositions and structures are similar: both are 2:1 clays, both have Mg^{2+} and Fe in their octahedral layers, and both have water in their interlayer sites. The spectral features discussed at length in this paper are not necessarily unique to vermiculite in that phyllosilicate minerals with the same octahedral layer cation clusters and interlayer water will produce absorptions with wavelength positions at or near those of vermiculite. Having stated this, there are some differences between the spectra of these saponite, vermiculite, and vermiculite ore samples. The spectrum of the unexpanded vermiculite has an overall wider set of overlapping overtone composite absorptions than that of the saponite (Fig. A16a; FWHM = 0.105 vs 0.087 μm, respectively). This may be due to a relatively higher water content of the vermiculite sample; however, the overall width of the overtone composite absorptions in the expanded vermiculite ore (composed of phlogopite, hydrobiotite, and vermiculite), with most of its interlayer water driven off by heating, is still wider (FWHM = 0.116 μm) than that in the saponite spectrum. The saponite spectrum lacks a distinct 1.38 μm absorption suggesting proportionately fewer repulsed Mg_3OH N-bands; however, the intermediate position of its 1.39 μm absorption suggests proportionately more non-repulsed Mg_3OH N-bands. Madejova (2003) lists two OH stretch absorptions for this saponite at 3717 and 3679 cm^{-1} with the latter about 5 times stronger than the former and close to the 3681 cm^{-1} position of the non-repulsed Mg_3OH:Si_5Al absorption in vermiculite. Based on compositional analysis of the SapCa-1 saponite by Post (1984), the tetrahedral Al/(Al+Si) of 0.06 is consistent with the presence of Mg_3OH:Si_5Al cation clusters. Likewise, the lack of a distinct 1.40 μm absorption in the saponite spectrum but presence of one at 1.41 μm may indicate proportionately fewer repulsed $(Mg,Fe^{2+})_2(Al,Fe^{3+})OH$ I-band absorptions but more non-repulsed $(Mg,Fe^{2+})_2(Al,Fe^{3+})OH$ I-band absorptions.

Spectral differences between combination absorptions in spectra of the vermiculite, the vermiculite ore, and saponite are more pronounced. The vermiculite spectrum (Fig. A16b) has a stronger 2.30 μm composite absorption than that of saponite. However, saponite's 2.38 μm composite absorption is stronger than the corresponding absorptions in spectra of the vermiculite and vermiculite ore. Saponite's spectrum lacks a distinct 2.32 μm absorption suggesting proportionately fewer repulsed Mg_3OH N-bands; however, the intermediate position of its 2.315 μm c_d N-band absorption suggests proportionately more non-repulsed Mg_3OH:Si_5Al cation clusters—consistent with the type of absorptions in its overtone region. Again, the overall width of the 2.315 μm composite absorption in saponite's spectrum is narrower than that of the 2.32 μm composite absorption in spectra of the vermiculite and vermiculite ore (i.e., FWHM = 0.044 μm versus 0.060 and 0.054 μm, respectively). The apparent weakness of repulsed N- and I-bands in saponite's spectrum may account for its narrower overtone and combination composite absorptions relative to those in the vermiculite ore's spectrum. The dominance of non-repulsed Mg_3OH:Si_5Al absorptions but lack of corresponding non-repulsed Mg_3OH:Si_2Al_4 absorptions in saponite's spectrum may account for its narrow overtone and combination composite absorptions relative to those of vermiculite. Alternatively, saponites with more tetrahedral Al may have spectral features that more closely resemble those of vermiculite, including a stronger 2.30 μm c_e composite absorption due to more abundant non-repulsed Mg_3OH:Si_4Al_2 cation clusters. In this regard, Al-rich saponites may provide a spectral match to the "Fe/Mg smectites" identified on the Martian surface. Interested researchers could use cation-exchange experiments to test these assignments (i.e., repulsed absorptions intensify while non-repulsed absorptions diminish) to further our understanding of the spectral differences between these minerals.

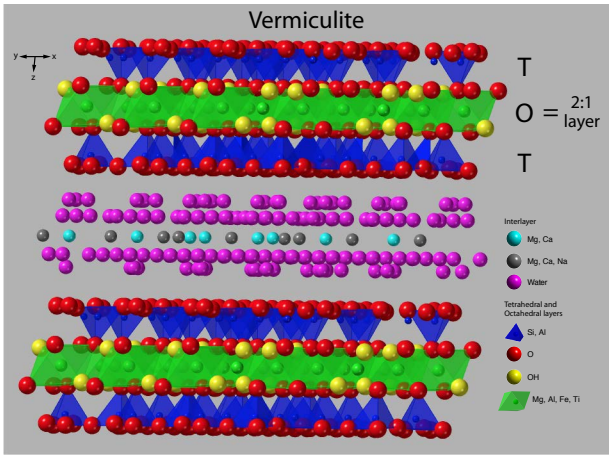

FIGURE A1. Atomic structure model of a vermiculite from Santa Olalla, Teoledo Province, Spain, based on X-ray diffraction information from Arguelles et al. (2010), created using CrystalMaker® v. 10.0.4. It consists of octahedral layers (O) sandwiched between tetrahedral layers (T) forming repeating T-O-T stacks that surround water-rich interlayers forming a 2:1 clay.

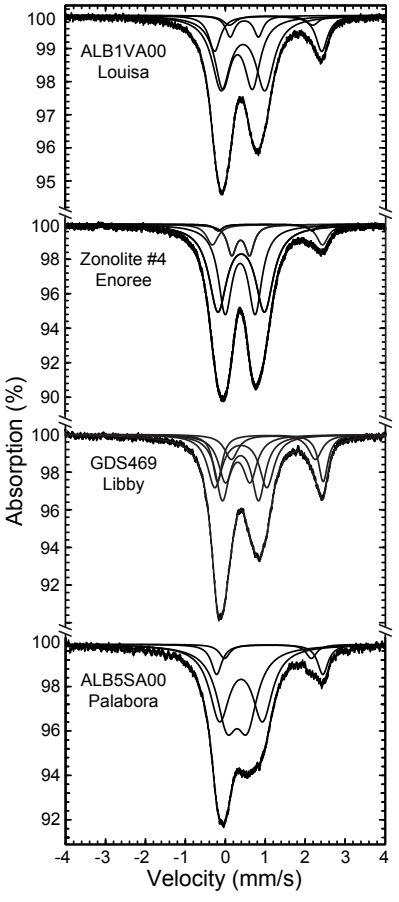

FIGURE A2. The 295 K Mössbauer spectra of selected unexpanded vermiculite ore samples from the four major historical sources. See text for a discussion of the deconvolution modeling process.

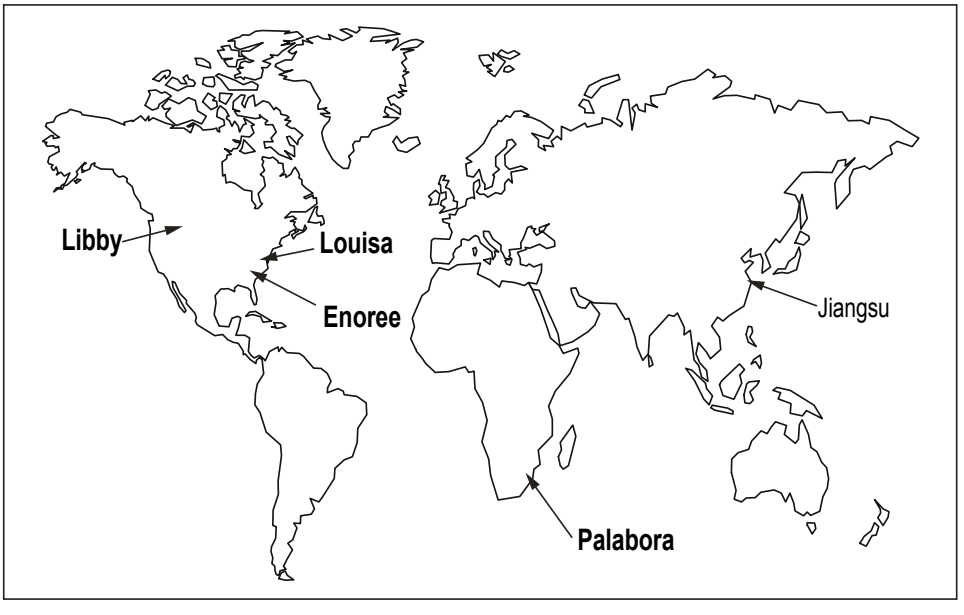

FIGURE A3. Locations of the four major historical vermiculite ore sources (in bold) for the U.S. market including Libby, Montana; Louisa, Virginia; Enoree district, South Carolina; and Palabora, South Africa. An expanded vermiculite ore sample from Jiangsu, China was also part of this study. Modified from Frank and Edmond (2001).

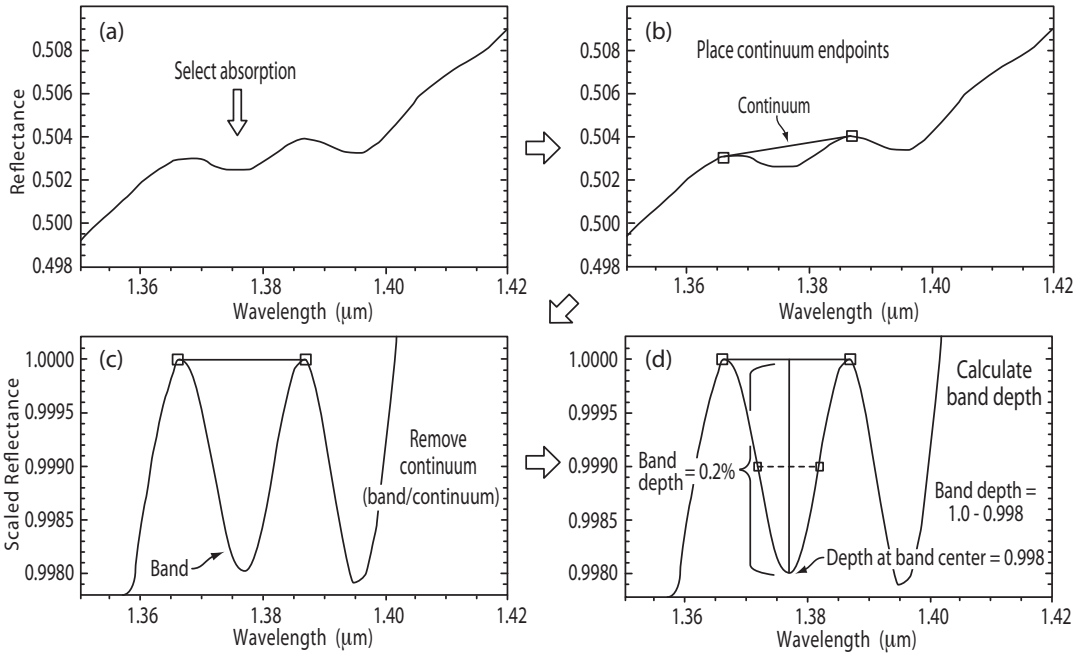

FIGURE A4. Spectral absorption continuum removal procedure. Note continuum endpoints were manually selected in this study, but their selection could be automated using first derivatives to locate shoulder high points in high signal-to-noise ratio reflectance data. See appendix discussion for details of this procedure.

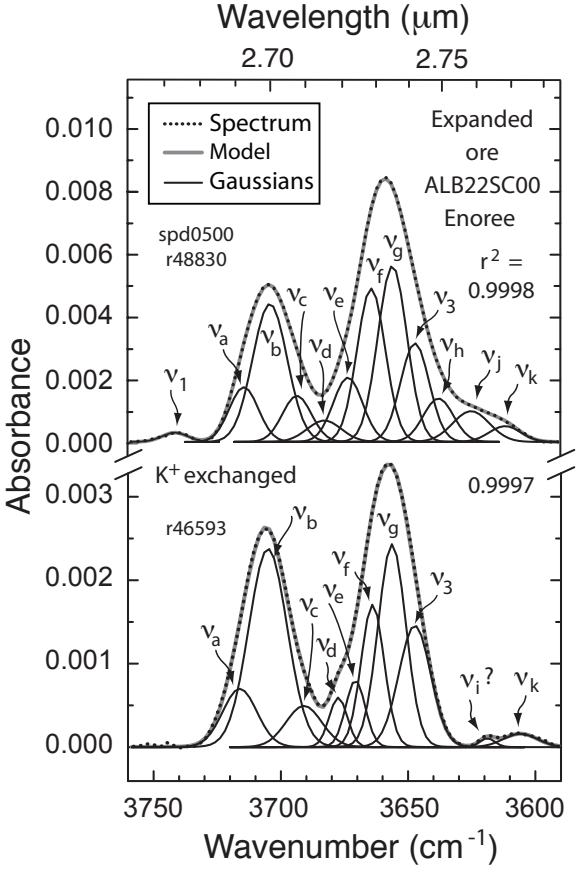

FIGURE A5. Continuum-removed absorbance spectra of the expanded ALB22SC00 ore sample from Enoree, before and after K^+ exchange, in the OH stretch fundamental region showing absorptions and their deconvolution into symmetrical Gaussians. Note that the ν_3 MgAl□OH absorption retains its strength relative to the ν_g non-repulsed I-band absorption after K^+ exchange. Vibrational assignments for the absorptions are given in Table 5. The coefficient of determination (r^2) gives the goodness of fit between the observed spectrum (dotted line) and deconvolution model (wide gray line under dotted line).

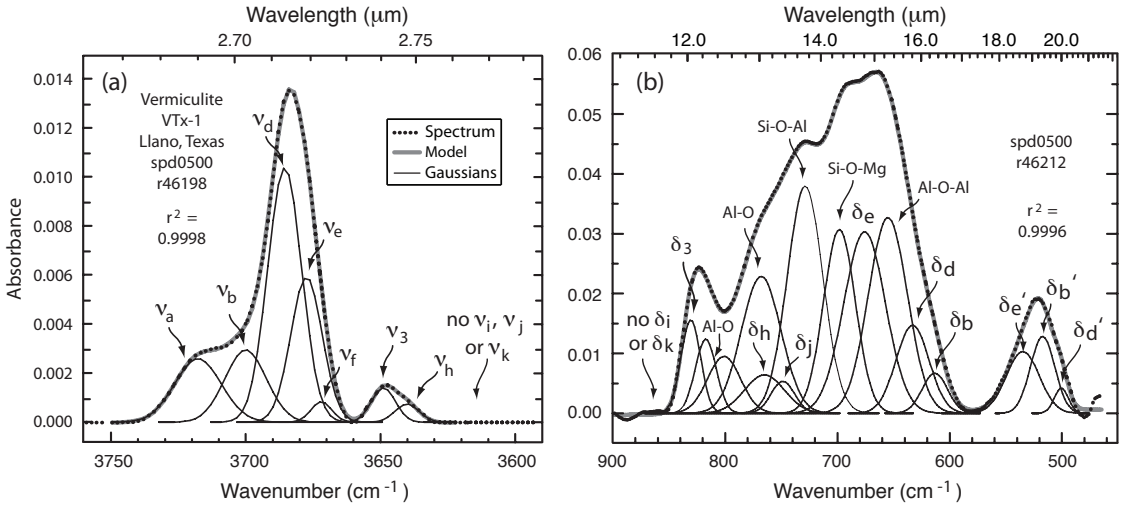

FIGURE A6. Continuum-removed absorbance spectra of an unexpanded Mg-vermiculite VTx-1 sample from Llano, Texas, in the (**a**) OH stretch and (**b**) cation-OH bend fundamental regions showing absorptions and their deconvolution into symmetrical Gaussians. Vibrational assignments for the absorptions are given in Table 5. The need to tie a continuum endpoint to the low-frequency side of the broad 600 to 850 cm^{-1} composite absorption in the presence of strong overlapping H_2O-related absorptions, distorts the relative strength of δ_d, which is actually greater than that of δ_e, whereas the relative strength of δ_a (not shown) is actually about equal to that of δ_b. The coefficient of determination (r^2) gives the goodness of fit between the observed spectrum (dotted line) and deconvolution model (wide gray line under dotted line).

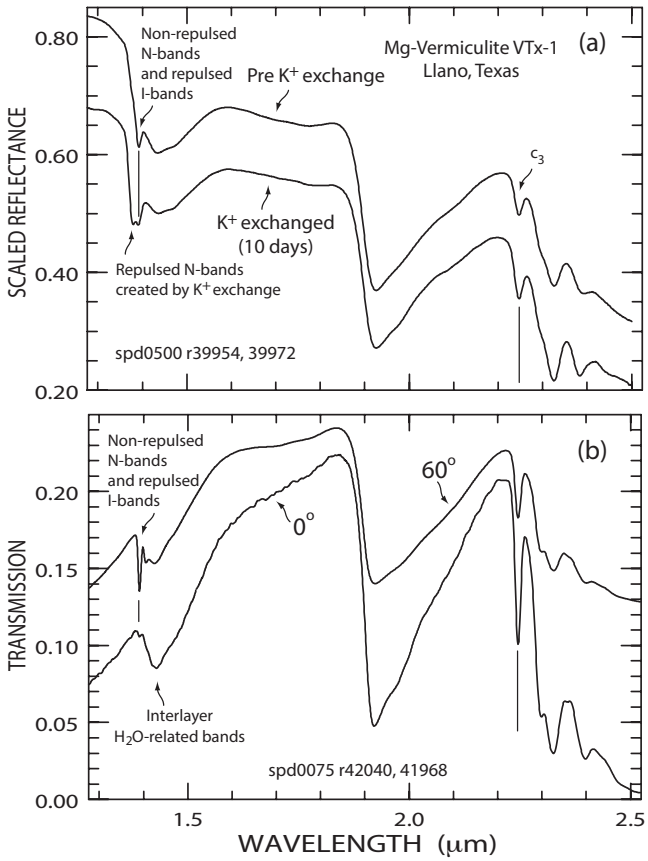

FIGURE A7. (**a**) NIR reflectance spectra of the unexpanded Mg-vermiculite VTx-1 sample from Llano, Texas, before and after K^+ exchange. Note the 2.24 μm c_3 composite combination absorption persists even after K^+ replaces interlayer water. (**b**) Polarized transmission spectra of VTx-1 showing that the intensity of the 2.24 μm absorption is stronger when light is parallel to the basal cleavage (inclination = 0°), whereas the 1.39 μm composite absorption (marked by leftmost vertical lines) is weaker. See appendix for a discussion of the significance of these observations. Rightmost vertical lines mark position of the 2.24 μm absorption. Reflectance spectra offset vertically for clarity.

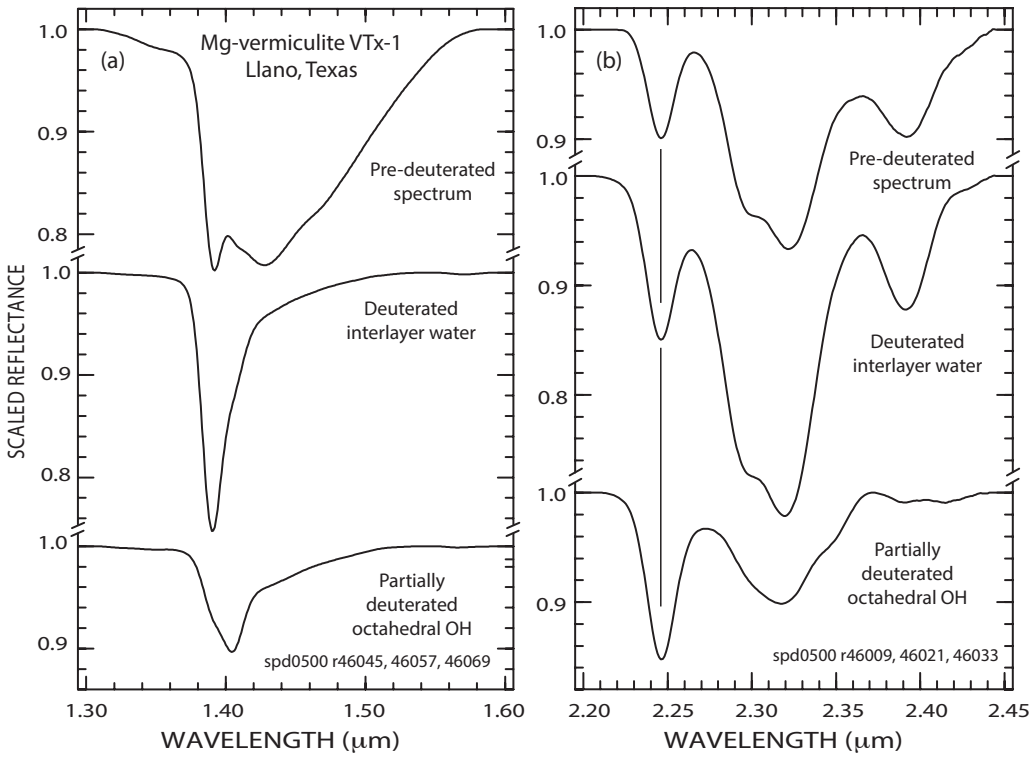

FIGURE A8. Continuum-removed (**a**) OH stretch overtone and (**b**) combination absorptions of the Mg-vermiculite VTx-1 sample from Llano, Texas, before and after partial deuteration. In the middle spectra, H_2O absorptions are replaced by D_2O absorptions at longer wavelengths (not shown), which reduces overlap with the 1.4 μm region OH overtone and 2.3 μm region combination absorptions. Weaker H_2O absorptions, as a result of deuteration, allow photons to penetrate further into the sample, so the OH absorptions become stronger relative to those in spectra of the pre-deuteration sample, after continuum removal. Vertical lines mark the wavelength position of the 2.24 μm absorption.

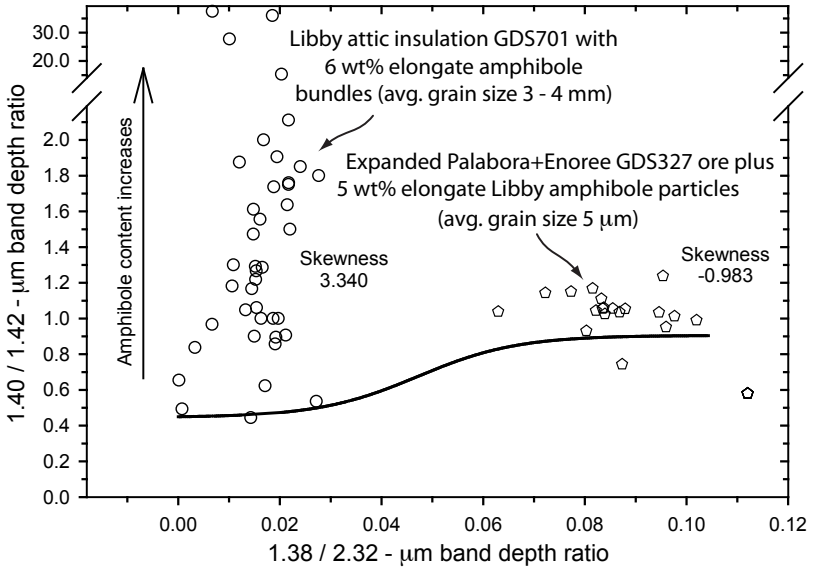

FIGURE A9. The distribution of individual 1.40/1.42 μm band-depth-ratio values of expanded Libby vermiculite ore is positively skewed by the presence of coarse-grained elongate amphibole bundle impurities relative to the negative skew of band-depth-ratio values of an expanded Palabora – Enoree ore mixture that was amended with fine-grained elongate amphibole particles. Black curve is the impurity non-detect threshold (see text for more details).

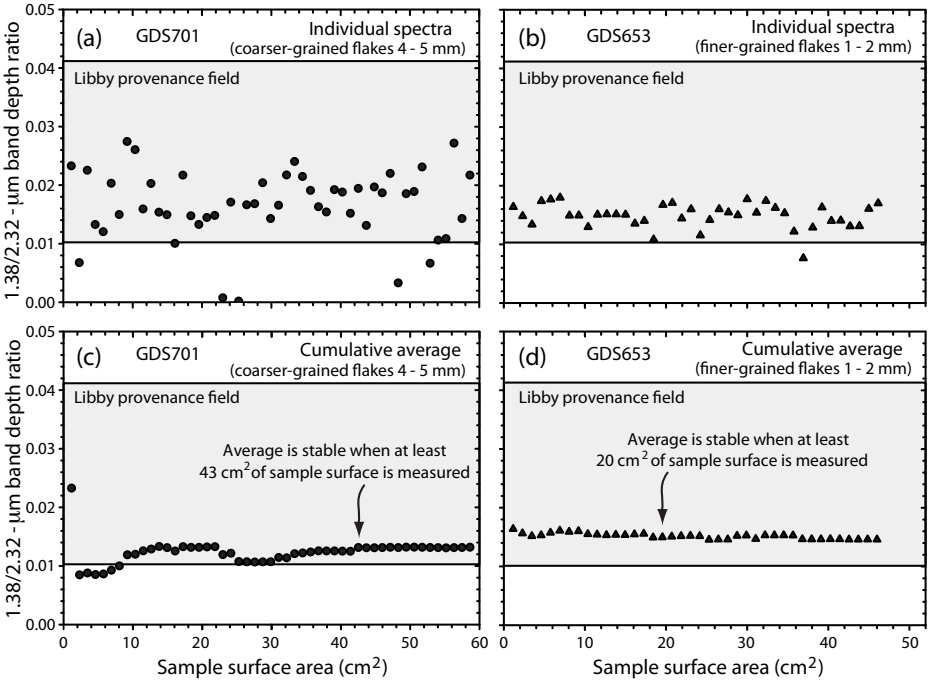

FIGURE A10. Evaluation of the total surface area of an expanded vermiculite ore sample that must be spectrally measured to derive a precise average 1.38/2.32 µm band-depth-ratio value for source determination. Individual measurements of 1.38/2.32 µm band-depth-ratio values for expanded Libby ore samples with different average flake size distributions: (**a**) 4 to 5 mm and (**b**) 1 to 2 mm. Note that some individual band-depth-ratio values fall outside the Libby provenance field. (**c** and **d**) Cumulative averages of 1.38/2.32 µm band-depth-ratio values for the same samples. Variability in the cumulative average band-depth-ratio values stabilize after measuring 43 cm^2 of the coarser-grained sample's surface area, whereas only 20 cm^2 must be measured to reach stable values for the finer-grained sample.

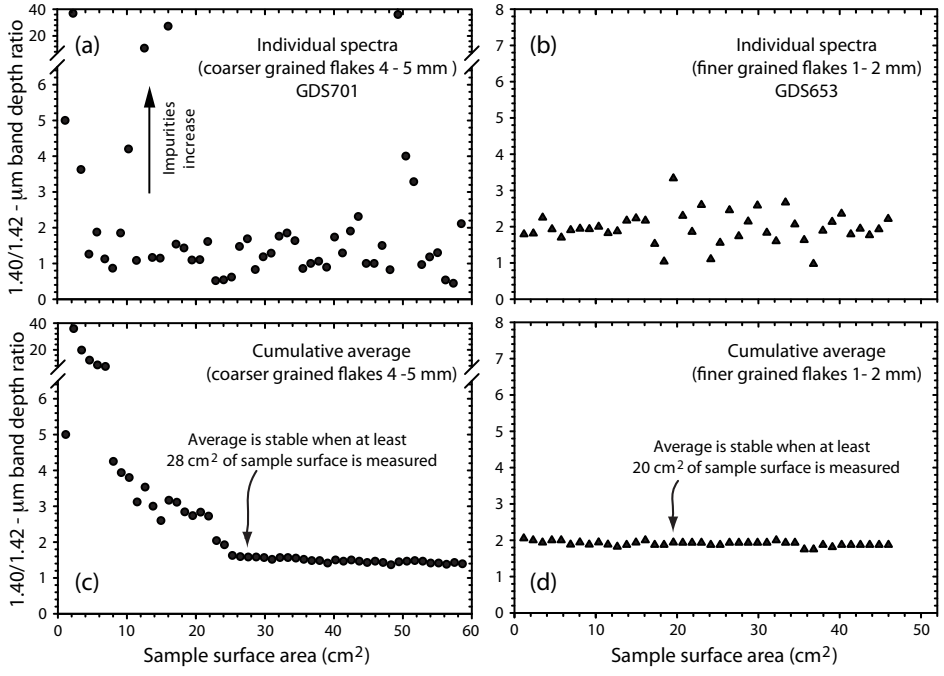

FIGURE A11. Evaluation of the total surface area of an expanded vermiculite ore sample that must be spectrally measured to derive a precise average band-depth-ratio value for detecting amphibole, talc, and/or serpentine impurities. (**a** and **b**) Individual measurements of 1.40/1.42 µm band-depth-ratio values for coarser- and finer-grained expanded Libby ore samples. (**c** and **d**) Cumulative averages of 1.40/1.42 µm band-depth-ratio values for the same samples. Band-depth-ratio values stabilize after measuring 28 cm^2 of the coarser-grained sample's surface area whereas only 20 cm^2 must be measured to reach stable values for the finer-grained sample.

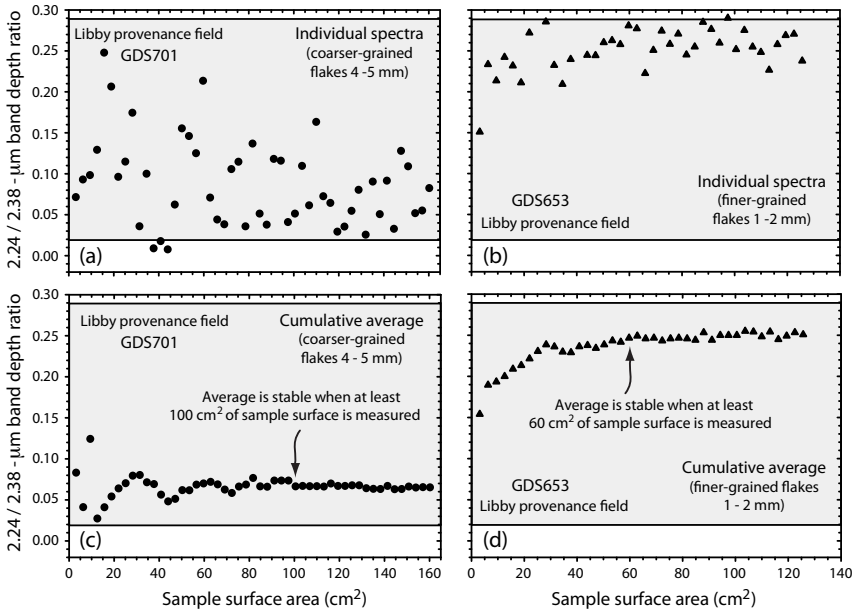

FIGURE A12. Evaluation of the total surface area of an expanded vermiculite ore sample that must be spectrally measured to derive a precise average 2.24/2.38 µm band-depth-ratio value for source determination. (**a** and **b**) Individual measurements of 2.24/2.38 µm band-depth-ratio values for coarser- and finer-grained expanded Libby ore samples. Note that some individual data values fall outside the Libby provenance field. (**c** and **d**) cumulative averages of 2.24/2.38 µm band-depth-ratio values for the same samples. Band-depth-ratio values stabilize after measuring 100 cm^2 of the coarser-grained sample's surface area whereas only 60 cm^2 need be measured to reach stable values for the finer-grained sample.

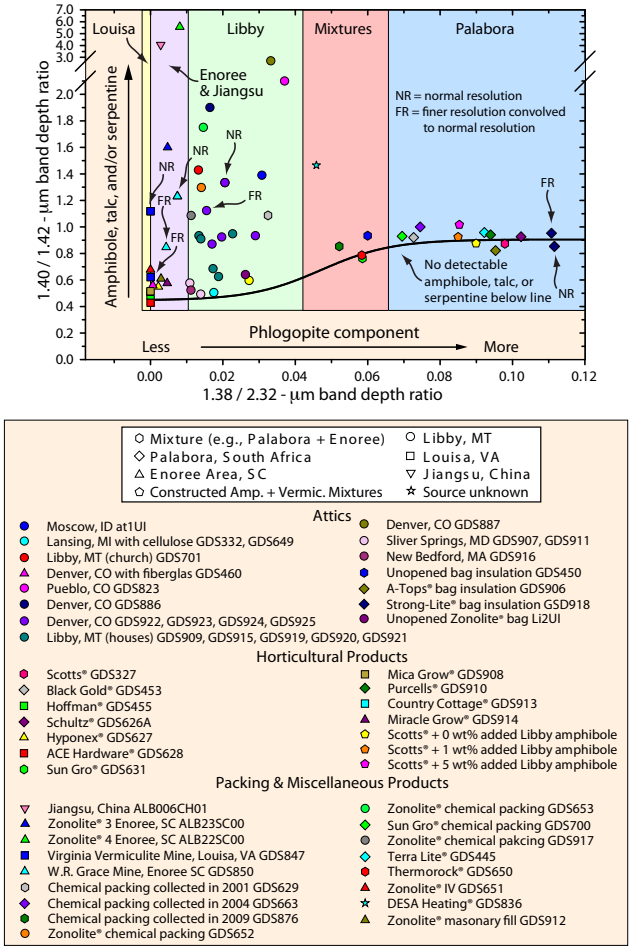

FIGURE A13. Same as Figure 16 with band-depth-ratio values of a few expanded vermiculite ore samples derived from spectra measured at finer spectral resolution (6 nm) then convolved to the sampling and bandpasses of the normal resolution (11 nm). FR= band-depth-ratio values from the convolved finer resolution spectra; NR = band-depth-ratio values from the spectra measured at normal resolution. Note that FR points plot within their correct provenance fields. An ASD FieldSpec 4 Hi-Res NG® spectrometer was used to measure the reflectance of the samples at 6 nm resolution.

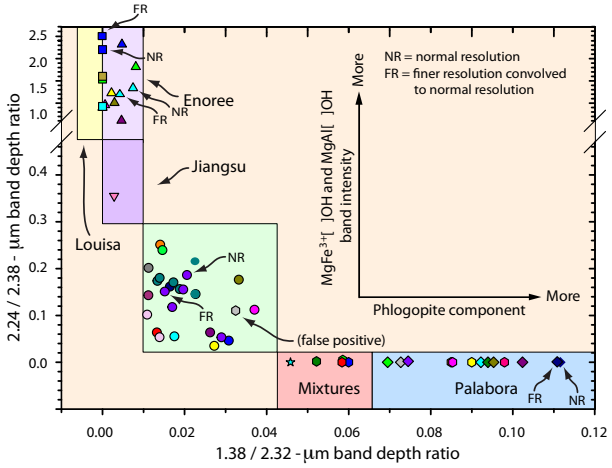

FIGURE A14. Same as Figure 18 with band-depth-ratio values of a few expanded vermiculite ore samples derived from spectra measured at finer spectral resolution (6 nm) then convolved to the sampling and bandpasses of the normal resolution (11 nm). FR= band-depth-ratio values from the convolved finer resolution spectra; NR = band-depth-ratio values from the spectra measured at normal resolution. Note that FR points plot within their correct provenance fields. An ASD FieldSpec 4 Hi-Res NG® spectrometer was used to measure the reflectance of samples at 6 nm resolution.

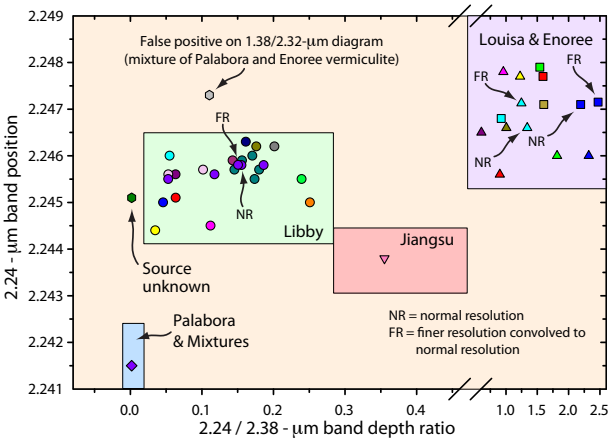

FIGURE A15. Same as Figure 21 with 2.24/2.38 µm band depth ratio and 2.24 µm absorption wavelength position values of a few expanded vermiculite ore samples derived from spectra measured at finer spectral resolution (6 nm) then convolved to the sampling and bandpasses of the normal resolution (11 nm). FR= band-depth-ratio values from the convolved finer resolution spectra; NR = band-depth-ratio values from the spectra measured at normal resolution. Note that FR points plot within their correct provenance fields. An ASD FieldSpec 4 Hi-Res NG® spectrometer was used to measure the reflectance of samples at 6 nm resolution.

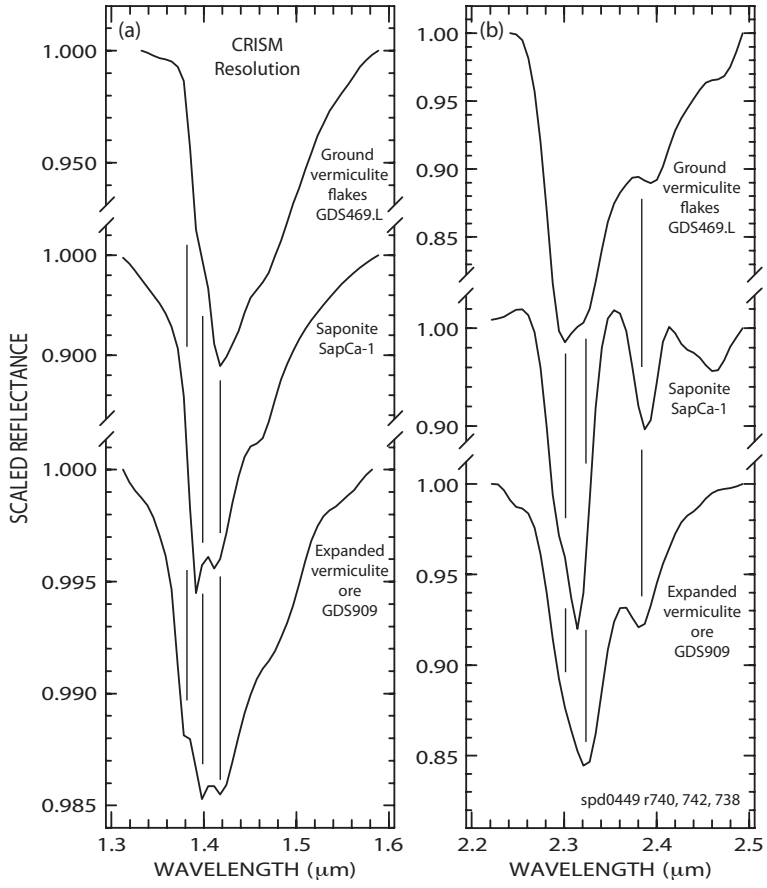

FIGURE A16. Continuum-removed reflectance spectra of vermiculite, saponite, and expanded vermiculite ore showing absorptions in the NIR (**a**) overtone and (**b**) combination spectral regions. All spectra are convolved to CRISM (Compact Reconnaissance Imaging Spectrometer for Mars) spectral resolution (Mustard et al. 2008). Vertical lines in (**a**) mark the wavelength positions of the 1.38, 1.40, 1.42 µm composite overtone absorptions in the spectrum of the vermiculite ore; vertical lines in (**b**) mark the 2.30, 2.32, and 2.38 µm composite combination absorptions in spectra of the vermiculite and vermiculite ore. Spectral identification numbers (i.e., spd0449 r740) uniquely identify spectra. Vermiculite and expanded vermiculite ore samples are from this study. Saponite SapCa-1 is from the Source Clays Repository with its chemistry listed in Post (1984). This sample underwent acetate-acetic acid buffer removal of carbonate prior to spectral measurement.